Available online at www.sciencedirect.com
SCIENCE DIRECT
Journal of Power Sources 157 (2006) 45–55
JOURNAL OF POWER SOURCES
www.elsevier.com/locate/jpowsour

Tailoring a Pt–Ru catalyst for enhanced methanol electro-oxidation

R.K. Raman [a], A.K. Shukla [a,d,*], A. Gayen [a], M.S. Hegde [a], K.R. Priolkar [b], P.R. Sarode [b], S. Emura [c]

[a] *Solid State and Structural Chemistry Unit, Indian Institute of Science, Bangalore 560012, India*
[b] *Department of Physics, Goa University, Taleigao Plateau, Goa 403206, India*
[c] *Institute of Scientific and Industrial Research, Osaka University, Mihoga-Oka 8-1, Ibaraki, Osaka 567-0047, Japan*
[d] *Central Electrochemical Research Institute, Karaikudi 630006, Tamilnadu, India*

Accepted 30 June 2005
Available online 19 August 2005

Abstract

A carbon-supported (1:1) Pt–Ru (Pt–Ru/C) alloy catalyst has been prepared in-house by the sulfito-complex route, and has been tailored to achieve enhanced activity towards methanol electro-oxidation by annealing it at varying temperatures in air. The catalyst samples annealed between 250 and 300 °C in air for 30 min exhibit superior catalytic activity towards methanol electro-oxidation in a solid-polymer-electrolyte direct methanol fuel cell (SPE-DMFCs) operating at 90 °C. Both the as-prepared and annealed Pt–Ru/C catalysts have been characterized by powder X-ray diffraction (XRD), transmission electron microscopy (TEM), X-ray photoelectron spectroscopy (XPS), extended X-ray absorption fine structure (EXAFS), and cyclic voltammetry. It is conjectured that while annealing the Pt–Ru/C catalysts, both Pt–Pt and Pt–Ru bonds increase whereas the Pt–O bond shrinks. This is accompanied with a positive variation in Ru/Pt metal ratio suggesting the diffusion of Ru metal from the bulk catalyst to surface with an increase in oxidic ruthenium content. Such a treatment appears seminal for enhancing the electrochemical activity of Pt–Ru catalysts towards methanol oxidation.

Keywords: Methanol electro-oxidation; Direct methanol fuel cell; Electron microscopy; Photoelectron spectroscopy; X-ray absorption spectroscopy

1. Introduction

At present, methanol is the most attractive organic liquid-fuel for directly fueled polymer electrolyte fuel cells (PEFCs) [1]. Directly methanol-fueled PEFCs are called solid-polymer-electrolyte direct methanol fuel cells (SPE-DMFCs), and are commercially attractive since the use of a liquid reactant at the front-end of the fuel cell simplifies engineering problems and hence its cost. In the literature, although a variety of methanol oxidation catalysts have been attempted, Pt–Ru/C alloy indisputably remains the most potential catalyst and efforts are being expended to further their activity [2].

During methanol oxidation, three quite different electrochemical reactions occur. The first is a dissociative chemisorption of the alcohol onto the surface, which involves successive donation of electrons to the catalyst as depicted below:

$$\mathrm{Pt} + \mathrm{CH_3OH} \xrightarrow{k_1} \mathrm{Pt{-}CH_2{-}OH} + \mathrm{H_{ads}} \quad (1)$$

$$\mathrm{Pt} + \mathrm{Pt{-}CH_2{-}OH} \xrightarrow{k_2} \mathrm{Pt_2{=}CH{-}OH} + \mathrm{H_{ads}} \quad (2)$$

$$\mathrm{Pt} + \mathrm{Pt_2{=}CHOH} \xrightarrow{k_3} \mathrm{Pt_3{\equiv}C{-}OH} + \mathrm{H_{ads}} \quad (3)$$

where $k_1 < k_2 < k_3$ makes Pt_3–COH the major surface species. H_{ads} is lost to the solution as H^+ according to:

$$\mathrm{H_{ads}} \leftrightarrow \mathrm{Pt{-}H} \rightarrow \mathrm{Pt} + \mathrm{H^+} + \mathrm{e^-} \quad (4)$$

In a Pt–Ru catalyst, Ru would promote the initial steps of this reaction. However, capture of the surface protons and

* Corresponding author. Tel.: +91 80 22932795; fax: +91 80 2360 13 10.
E-mail address: shukla@sscu.iisc.ernet.in (A.K. Shukla).

0378-7753/$ – see front matter © 2005 Elsevier B.V. All rights reserved.
doi:10.1016/j.jpowsour.2005.06.031

the COH^- radical by negatively charged surface metal atoms would inhibit their desorption. The subsequent electrochemical reaction involves attraction of an oxygen species from the aqueous electrolyte to the catalyst surface as follows:

$$Ru + H_2O \rightarrow Ru{-}OH + H^+ + e^- \quad (5)$$

The final electrochemical reaction is the following two-step process:

$$Ru{-}OH \rightarrow Ru{-}O + H^+ + e^- \quad (6)$$

$$Ru{-}O + Pt_3{-}COH \rightarrow Ru + 3Pt + CO_2 \uparrow + H^+ + e^- \quad (7)$$

Of these, the first step is promoted by a charge transfer from Ru to Pt sites in the catalyst [3]. From the foregoing, it is surmised that both the physical and chemical compositions of the carbon-supported Pt–Ru catalyst are seminal for its activity towards electro-oxidation of methanol [3,4].

In this communication, we have employed powder X-ray diffraction, electron microscopy, X-ray photoelectron spectroscopy and extended X-ray absorption fine structure in conjunction with electrochemistry, to tailor a carbon-supported Pt–Ru (Pt–Ru/C) alloy catalyst so as to achieve the enhanced methanol oxidation activity.

2. Experimental

2.1. Preparation of carbon-supported platinum-ruthenium (Pt–Ru/C) catalysts

Sulfito-complex route was adopted to prepare 60 wt.% Pt–Ru/C [2]. In brief, the required amounts of $Na_6[Pt(SO_3)_4]$ and $Na_6[Ru(SO_3)_4]$ were dissolved in dilute sulphuric acid solution, which was then added drop wise to the beaker containing deionized water with constant stirring. While adding these complexes, 30% H_2O_2 was added simultaneously to decompose the sulfito-complexes of Pt and Ru. During this reaction, the pH of the solution was maintained at ~5 using dilute aqueous NaOH solution to keep oxides of Pt and Ru in colloidal phase. The required amount of Vulcan-XC 72R carbon was suspended in distilled water and agitated in an ultrasonic water bath to form slurry. Subsequently, the carbon slurry was added in the colloidal bath while maintaining its pH at ~5 to deposit Pt and Ru oxides over carbon. After the complete decomposition of excess peroxide added, H_2 gas was bubbled vigorously to reduce the Pt and Ru oxides into Pt–Ru solid-solution deposited over carbon, which was filtered, washed copiously with hot distilled water, and dried in an air oven at 80 °C for 2 h. The catalyst thus obtained was heat treated at varying temperatures between 200 and 300 °C in air for half an hour.

2.2. Physical characterization Pt–Ru/C catalysts

Powder X-ray diffraction (XRD) patterns for various Pt–Ru/C catalysts were recorded on a Siemens D-5005 X-ray diffractometer using Cu Kα radiation. Transmission electron microscope (TEM) images and Electron diffraction (ED) patterns of Pt–Ru/C catalysts were recorded on JEOL JEM-2000FX II. X-ray photoelectron spectra (XPS) of Pt–Ru/C catalysts were recorded on an ESCA-3 Mark II spectrometer (VG Scientific Ltd., England) using Al Kα radiation (1486.6 eV) at pass energy of 50 eV. Binding energies calibrated with respect to C(1s) at 284.6 eV were accurate within ±0.2 eV and there was no charging in any of the samples as they were conducting. For XPS analysis, the powder samples were made into pellets of 8 mm diameter and placed in an ultra high vacuum chamber at 10^{-9} Torr housing the analyzer. Prior to mounting the sample in the analyzing chamber, the samples were kept in the preparation chamber at 10^{-9} Torr for 5 h in order to desorb any volatile species present on the catalyst. The experimental data were curve fitted with Gaussian peaks after subtracting the linear background. For Gaussian peaks a slightly different full-width at half-maximum (FWHM) value was used for different chemical states. The spin–orbit splitting and the doublet intensities were fixed as described in the literature. The surface concentration of different states was estimated from the areas of the respective Gaussian peaks.

Extended X-ray absorption fine structure (EXAFS) data were collected using a double crystal (Si(3 1 1)) spectrometer. The energy was calibrated using the first inflection point of Pt L_{III} edge in a Pt metal foil (Pt L_{III} edge = 11.56 keV). The absorbers were made by pressing the samples into pellets of 10 mm diameter with boron nitride as binder. To avoid the sample thickness effect, $\Delta\mu_0 x$ was restricted to a value ≤ 1 by adjusting the thickness of the absorber pellet, where $\Delta\mu_0$ is the edge step in the absorption coefficient and x is the sample thickness [5]. The X-ray energy was scanned with respect to Pt-edge EXAFS from −300 eV to about 1000 eV with respect to Pt L_{III} edge energy. The normalized EXAFS function $\chi(k)$ is given by:

$$\chi(k) = \frac{\mu(k) - \mu_0(k)}{\Delta\mu_0} \quad (4')$$

where $\mu(k)$ is the measured absorption, $\mu_0(k)$ is the background absorption, $\Delta\mu_0$ is the edge step, and k is the wave vector given by, $(2m(E - E_0)/\hbar^2)^{1/2}$, where m, $\hbar$, E, E_0 are mass of the electron, Planck's constant, X-ray energy and threshold energy associated with the ejection of the electron, respectively. The value of E_0 is estimated from the first inflection point found in the derivative of Pt L_{III} edge absorption spectrum of each compound, which is used as an input parameter for background subtraction. In order to obtain information about individual shells Fourier transform (FT) of EXAFS function, $\chi(k)$ to R-space was performed between 3 and 15 $Å^{-1}$ using k^3-weighting and Hanning window function. The magnitude of FT, $\Phi(R)$ exhibits peaks at well-defined values of bond distances (R) corresponding to different coordination shells around the absorber atom. Structural parameters were obtained by fitting $\Phi(R)$ between 1 and 4 Å using FEFFIT program [6]. The theoretical calculations

of the back-scattering amplitude and phase-shift functions were obtained using FEFF (6.01) program [7]. The value of amplitude reduction factor (S_0^2) was deduced from EXAFS of Pt metal foil by using the degeneracy values calculated by FEFF for each cell. E_0 is one of the fitting parameters in FEFFIT program. Initially, it was taken as the energy corresponding to first inflection point in the derivative spectra of individual compounds. The goodness of the fit was estimated by means of χ^2, reduced-χ^2 and R factor. A fit with R factor $\leq$0.02 was taken as a good fit. From these analyses, structural parameters, namely coordination numbers (N), bond distance (R) and Debye–Waller factor (σ), have been calculated.

2.3. Electrochemical characterization of Pt–Ru/C catalyst

For the electrochemical characterization membrane electrode assemblies (MEAs) were obtained by sandwiching the pre-treated Nafion-117 polymer electrolyte membrane between the anode and cathode. Both the anode and cathode consist of backing layer, a gas-diffusion layer and a reaction layer. A teflonized (20 wt.% Teflon) carbon paper (Toray TGP-H-090) of 0.276 mm thickness was employed as the backing layer for the cathode, while unteflonized carbon paper was employed for anode. To prepare the gas diffusion layer, Vulcan-XC 72R carbon was suspended in cyclohexane and agitated in an ultrasonic water bath. To this, 13 wt.% Teflon (Fluon GP-2) suspension for cathode while 10 wt.% Nafion® ionomer in case of anode was added with continuous agitation. The required amount of cyclohexane was then added to it drop wise. The resultant slurry was spread onto respective carbon paper and dried in an air oven at 80 °C for 2 h. To prepare the reaction layer for cathode, the required amount of the catalyst (60 wt.% Pt/C) was suspended in isopropyl alcohol. The mixture was agitated in an ultrasonic water bath, and 10 wt.% Nafion® solution was added to it with continuing agitation for 1 h. The ink thus obtained was coated onto the gas-diffusion layer of the electrode, which was kept identical for all the MEAs. Anodes were made in a similar manner using commercial Pt–Ru/C (Johnson–Matthey), Pt–Ru/C as-prepared and the same air annealed separately at 200, 250 and 300 °C for half an hour. All the anodes and cathodes contained 60 wt.% Pt–Ru/C catalyst and 60 wt.% Pt/C each with a platinum loading of 1 mg cm^{-2}. A Nafion® loading of 0.25 mg cm^{-2} was provided to the surface of the electrodes. The membrane electrode assembly was obtained by hot pressing the cathode and anode on either side of a pre-treated Nafion®-117 membrane at 60 kg cm^{-2} at 125 °C for 3 min.

Liquid-feed SPE-DMFCs were assembled with the various MEAs. The anode and cathode of the MEAs were contacted on their rear with gas/fluid flow field plates machined from high-density graphite blocks in which channels were machined to achieve minimum mass-polarization in the SPE-DMFCs. The ridges between the channels make electrical contact with the back of the electrode and conduct the current to the external circuit. Electrical heaters were placed behind each of the graphite blocks to heat the cell to the desired temperature.

To study the methanol oxidation activity of various Pt–Ru/C catalysts, cyclic voltammetry on the catalyst electrodes was carried out in the fuel-cell configuration [8] employing an AutoLab PGSTAT-30 electrochemical system. A 2 M methanol solution was pumped to the anode chamber through a peristaltic pump and the unreacted solution was collected in the reservoir. A potential of 0.1 V versus standard hydrogen electrode (SHE) was applied for 1 h at 90 °C to ensure a monolayer methanol adsorption over the Pt–Ru/C catalyst, while passing H_2 gas at 1 atmosphere over cathode, which served both as the counter and reference electrodes. After 1 h, Millipore water was circulated for another 10 min to clean the excess methanol present in the anode chamber. The cycling was carried out between 0.1 and 0.8 V versus SHE. To maintain the humidity of the membrane, Millipore water was kept circulating through the cell [8]. To obtain anode polarization data, the cell was galvanostatically polarized at 90 °C, while passing 2 M methanol solution at anode. During this process hydrogen was evolved at the cathode, which served as a SHE [8].

3. Results and discussion

Powder X-ray powder diffraction patterns for Pt–Ru/C catalysts presented in Fig. 1 show all the characteristic peaks pertaining to face-centred cubic (fcc) crystallographic structure of Pt–Ru alloy [2]. The broad feature at a diffraction angle (2θ) ~25° can be attributed to (0 0 2) plane of the hexagonal structure for Vulcan XC-72R carbon [9]. A shift in the Pt peak position towards a higher angle is observed for Pt–Ru/C catalyst samples, confirming the formation of alloy phase between Pt and Ru [10]. TEM images of the as-prepared and 300 °C heat-treated Pt–Ru/C catalyst samples

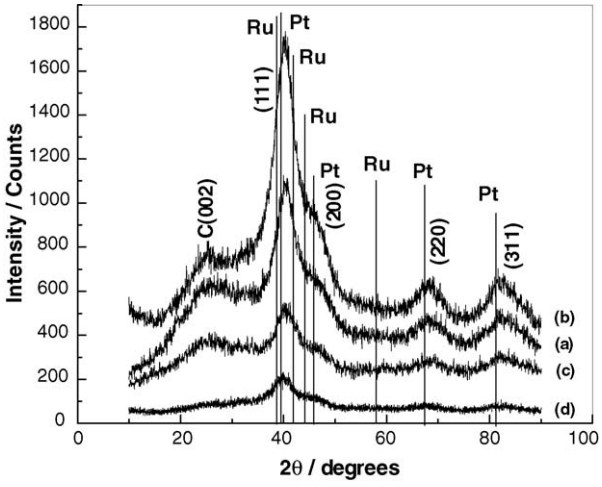

Fig. 1. X-ray powder diffraction patterns for (a) as-prepared Pt–Ru/C and subsequent to its annealing in air at (b) 200 °C; (c) 250 °C; (d) 300 °C.

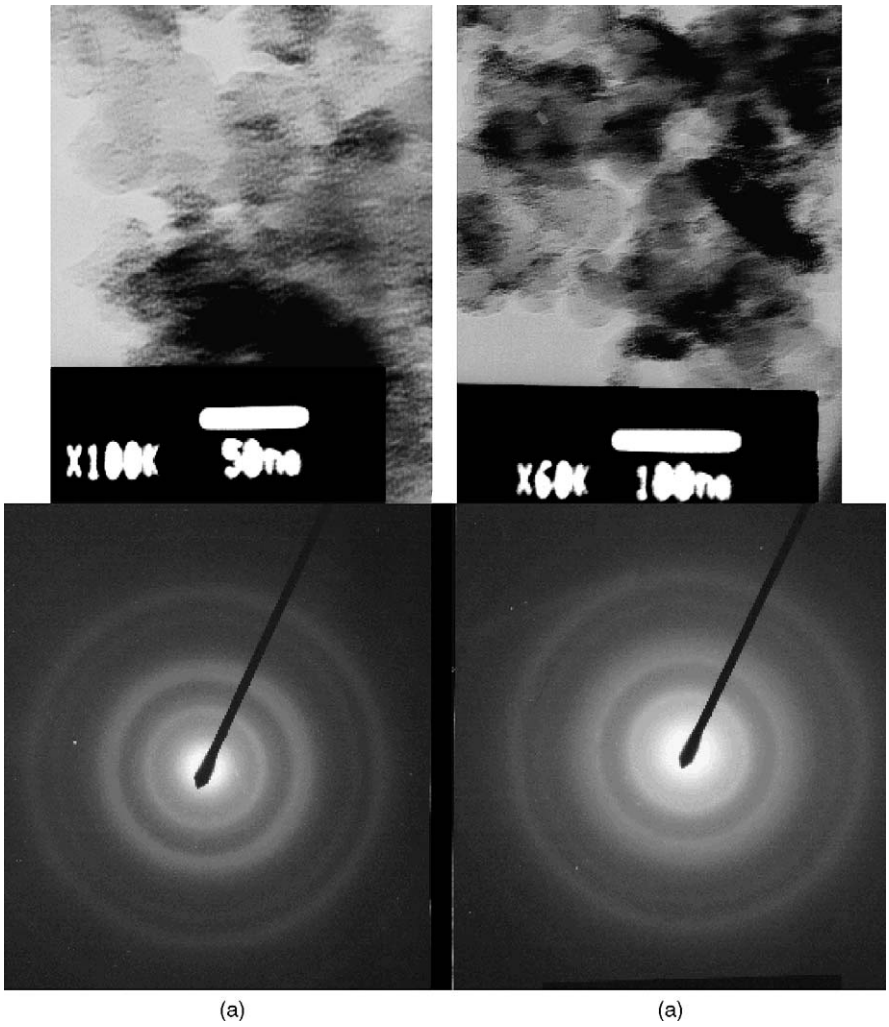

Fig. 2. TEM images and ED patterns for (a) as-prepared and (b) 300 °C treated Pt–Ru/C catalysts.

along with their ED patterns are shown in Fig. 2. The average particle size obtained from TEM analysis ranges between 10 and 20 Å. The *d*-spacing value of 2.25 Å calculated for (1 1 1) plane is in good agreement with the values derived from XRD patterns.

A comparison between in situ oxidative-stripping of adsorbed methanolic residues for the commercial, as-prepared and heat-treated Pt–Ru/C catalysts at 90 °C is depicted in Fig. 3. The electro-oxidation peak for methanolic residues on the as-prepared Pt–Ru/C catalyst sample appears at 0.35 V versus SHE while for the heat-treated and commercial Pt–Ru/C samples, it is observed at 0.25 V versus SHE. Accordingly, commercial Pt–Ru/C and heat-treated Pt–Ru/C catalysts oxidize the methanolic residues at a lesser overpotential in relation to as-prepared Pt–Ru/C catalyst. To evaluate the performance of Pt–Ru/C catalyst towards methanol oxidation in the fuel cell configuration, SPE-DMFCs were assembled with anodes of all Pt–Ru/C catalysts, and the anode polarization data was obtained as depicted in Fig. 4. It is observed that heat-treated Pt–Ru/C catalysts exhibit lower overpotential of ca. 150 mV at all load-

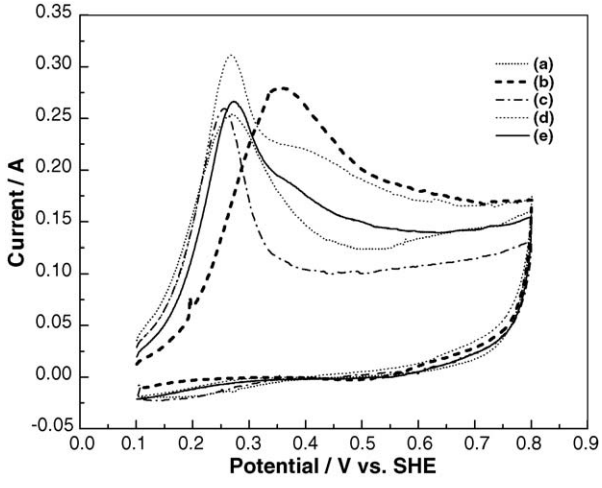

Fig. 3. In situ stripping voltammetry of methanol residues for (a) commercial Pt–Ru/C, (b) as-prepared Pt–Ru/C and as-prepared Pt–Ru/C after air annealing at (c) 200 °C; (d) 250 °C; (e) 300 °C at 90 °C (scan rate, 10 mV s^{-1}).

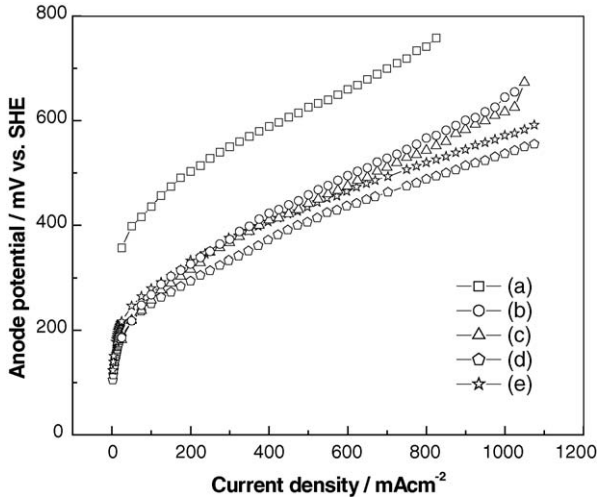

Fig. 4. Anode polarization data for the SPE-DMFCs which operating with 2 M aqueous methanol fuel at 90 °C employing membrane electrode assemblies with (a) as-prepared Pt–Ru/C, (b) commercial Pt–Ru/C, and as-prepared Pt–Ru/C after annealing it in air at (c) 200 °C; (d) 250 °C; (e) 300 °C.

current-densities in comparison to the as-prepared Pt–Ru/C catalyst. Although the initial overpotentials for methanol-oxidation at load current density ranging between 0 and 300 mA cm^{-2} for our heat-treated Pt–Ru/C samples are akin to commercial Pt–Ru/C sample, the former performs much better at load-current densities >350 mA cm^{-2}. To explain the increased activity of our heat-treated Pt–Ru/C catalysts towards methanol oxidation EXAFS and XPS studies have been conducted as described below.

Figs. 5 and 6 show Pt(4f) core level region for different Pt–Ru/C catalysts. The Pt(4f) region can be curve fitted to three sets of spin–orbit doublets. Accordingly, Pt($4f_{7/2,5/2}$) peaks at 71.4, 74.7; 72.8, 76.1 and 75.0, 78.2 eV have been assigned to Pt in 0, +2, and +4 states, respectively [11]. The full-width at the half-maximum (FWHM) values (Table 1) of the $4f_{7/2}$ peak for Pt^0, Pt^{2+} and Pt^{4+} are 2.0, 2.5, and 3.2 eV, respectively. The relative intensity of the different species obtained from the respective area is also listed in Table 1. Pt^0 is found to be the predominant species in all the catalysts. The Pt^0 percentage in commercial Pt–Ru/C is 46% while it is 44% in the catalyst prepared in-house. On heating the latter at 300 °C, it decreases to 40%. The surface concentration of Pt^{4+} remains constant at 21% while fraction of Pt^{2+} increases at the cost of Pt^0.

XPS of Ru(3d)–C(1s) region for various Pt–Ru/C samples are shown in Fig. 7. Since the C(1s) peak entirely covers the Ru($3d_{3/2}$) signal and partially overlaps with the Ru($3d_{5/2}$), a quantitative estimation of the oxidation states is not possible from these spectra. However, the peak at 280.5 eV with a shoulder at 281.6 eV can be qualitatively attributed to Ru^0 and anhydrous RuO_2, respectively [8]. The Ru($3d_{5/2}$) from hydrous amorphous $RuO_2{\cdot}xH_2O$ is expected at a binding energy ~1 eV higher than anhydrous RuO_2. Because of the overlap with the intense graphitic C(1s) peak, the presence of

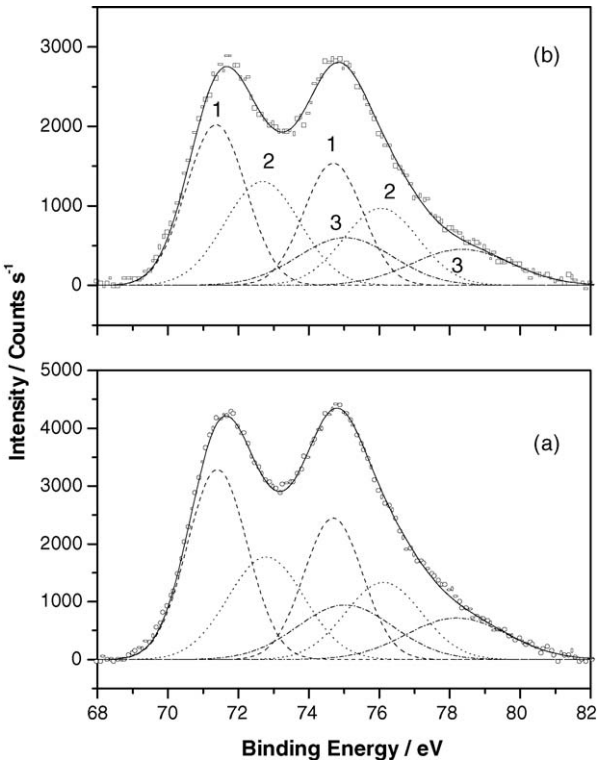

Fig. 5. X-ray photoelectron spectra for Pt(4f) region in (a) commercial Pt–Ru/C and (b) as-prepared Pt–Ru/C catalyst. The solid line represents the fitted XPS spectra, and the broken line represents the peaks due to platinum metal and its oxides (1, 2, 3 correspond to Pt^0, Pt^{2+}, and Pt^{4+}, respectively).

the hydrous ruthenium phase cannot be excluded. To avoid this, we undertook Ru($3p_{3/2}$) region to examine different Ru species and the deconvoluted spectra of different Pt–Ru/C catalysts are shown in Figs. 8 and 9. Fig. 8 also includes Ru($3p_{3/2}$) region (Fig. 8(c)) in pure RuO_2 for comparison. The parameters obtained from the analysis of the Ru($3p_{3/2}$)

Table 1
Binding energy (BE), FWHM, and relative intensity values for different Pt species as observed from Pt(4f) spectra for different Pt–Ru/C catalysts

Catalyst	Pt species	BE of $4f_{7/2}$ (eV)	FWHM (eV)	Relative intensity (%)
Pt–Ru/C (commercial)	Pt^0	71.4	2.0	46
	Pt^{2+}	72.9	2.5	32
	Pt^{4+}	75.0	3.2	22
Pt–Ru/C (as-prepared)	Pt^0	71.4	2.0	44
	Pt^{2+}	72.8	2.5	35
	Pt^{4+}	75.0	3.2	21
Pt–Ru/C (200 °C)	Pt^0	71.4	2.0	41
	Pt^{2+}	72.7	2.5	38
	Pt^{4+}	75.0	3.2	28
Pt–Ru/C (250 °C)	Pt^0	71.4	2.0	42
	Pt^{2+}	72.7	2.4	37
	Pt^{4+}	75.0	3.2	21
Pt–Ru/C (300 °C)	Pt^0	71.4	2.0	40
	Pt^{2+}	72.7	2.5	39
	Pt^{4+}	75.0	3.2	21

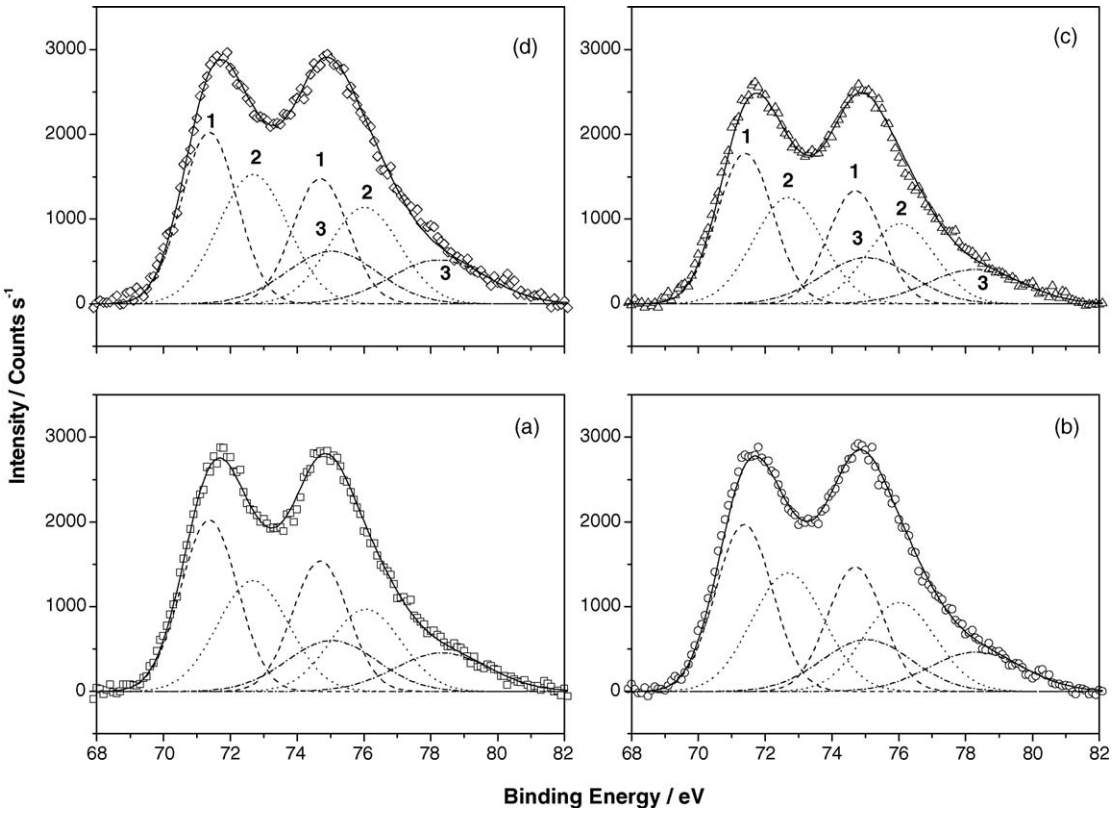

Fig. 6. X-ray photoelectron spectra for Pt(4f) region in (a) as-prepared Pt–Ru/C and as-prepared Pt–Ru/C after annealing it in air at (b) 200 °C; (c) 250 °C; (d) 300 °C. The solid line represents the fitted XPS spectra, and the broken line represents the peaks due to platinum metal and its oxides (1, 2, 3 correspond to Pt^0, Pt^{2+}, and Pt^{4+}, respectively).

region are listed in Table 2. The main Ru($3p_{3/2}$) peak in RuO_2 deconvoluted into a component observed at 463 eV and a higher binding energy component observed at 467.1 eV, which are ascribed to Ru^{4+} and hydrated Ru^{4+} species, respectively. By contrast, the Ru($3p_{3/2}$) peak in Pt–Ru/C catalysts deconvolutes at 461.3, 463.3, and 467.2 eV, which are attributed to Ru^0, anhydrous RuO_2, and hydrous amorphous $RuO_2{\cdot}xH_2O$, respectively [8]. The corresponding FWHM

Table 2
Binding energy, FWHM, and relative intensity values for different Ru species as observed from Ru(3p) spectra for RuO_2 and different Pt–Ru/C catalysts along with the surface concentrations of Ru to Pt

Catalyst	Ru species	BE of $3p_{3/2}$ (eV)	FWHM (eV)	Relative intensity (%)	X_{Ru}/X_{Pt}
RuO_2 (Fluka)	RuO_2	463.0	4.4	77	–
	$RuO_2{\cdot}xH_2O$	467.1	5.9	23	
Pt–Ru/C (commercial)	Ru^0	461.3	3.7	34	0.93
	RuO_2	463.5	4.1	45	
	$RuO_2{\cdot}xH_2O$	467.2	5.9	21	
Pt–Ru/C (as-prepared)	Ru^0	461.4	3.7	23	0.95
	RuO_2	463.4	4.1	53	
	$RuO_2{\cdot}xH_2O$	467.2	5.9	24	
Pt–Ru/C (200 °C)	Ru^0	461.3	3.7	23	0.94
	RuO_2	463.3	4.1	52	
	$RuO_2{\cdot}xH_2O$	467.2	5.9	25	
Pt–Ru/C (250 °C)	Ru^0	461.3	3.7	20	1.00
	RuO_2	463.4	4.0	56	
	$RuO_2{\cdot}xH_2O$	467.2	5.9	24	
Pt–Ru/C (300 °C)	Ru^0	461.3	3.7	18	0.95
	RuO_2	463.3	4.0	57	
	$RuO_2{\cdot}xH_2O$	467.2	5.9	25	

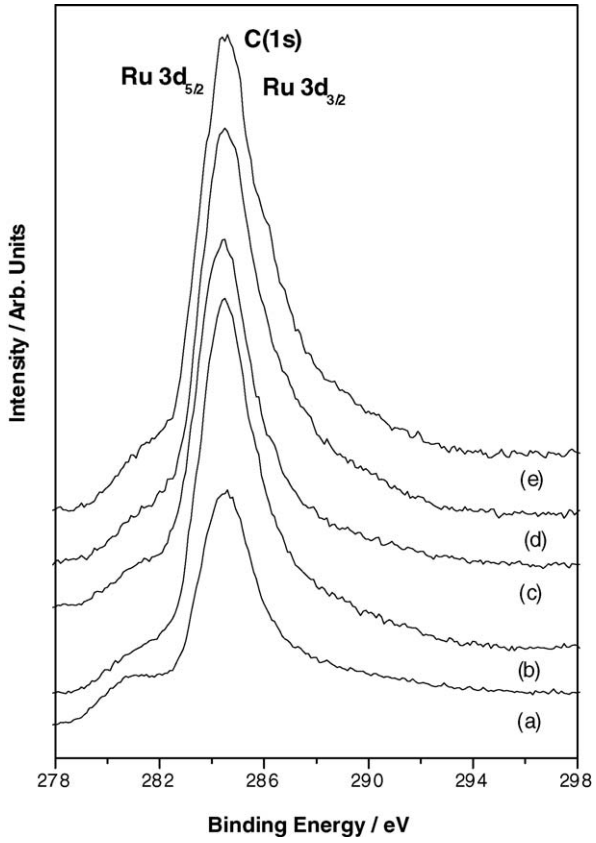

Fig. 7. C(1s) + Ru(3d) region in (a) commercial Pt–Ru/C, (b) as-prepared Pt–Ru/C and as-prepared Pt–Ru/C after annealing it in air at (c) 200 °C; (d) 250 °C; (e) 300 °C.

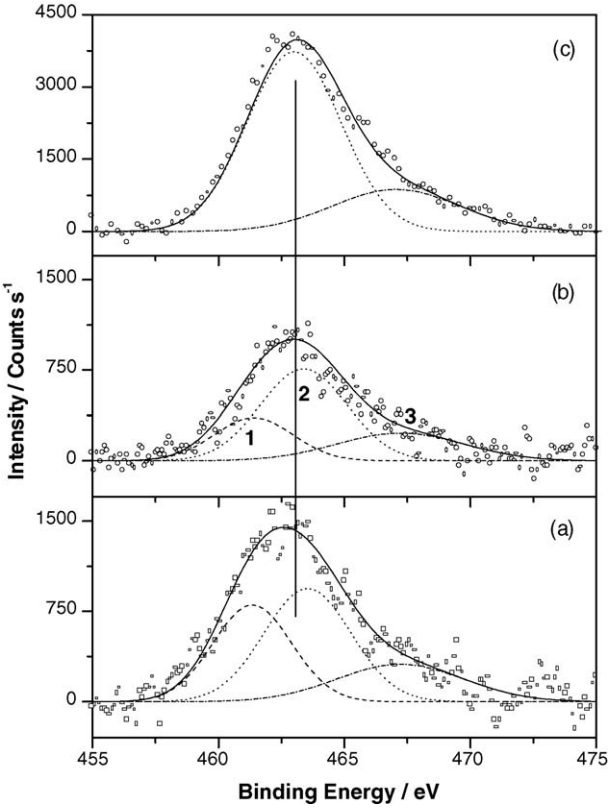

Fig. 8. Ru($3p_{3/2}$) region in (a) commercial Pt–Ru/C, (b) as-prepared Pt–Ru/C and (c) RuO_2 (1, 2, 3 correspond to Ru^0, RuO_2, and $RuO_2{\cdot}xH_2O$, respectively).

values of 3.7, 4.1, and 5.9 eV are for the metallic Ru and the two of its oxide phases, respectively. A comparison between RuO_2 and as-prepared Pt–Ru/C shows that oxidized Ru component is higher in the as-prepared catalyst in relation to commercial catalyst. The presence of RuO_3 phase was excluded in favour of the hydrous amorphous $RuO_2{\cdot}xH_2O$, since the former is thermodynamically unstable under the reaction conditions employed here [12]. It is noteworthy that the fraction of oxidized Ru is more in the in-house made and heat-treated catalysts in comparison to the commercial catalyst. While, Ru^0 percentage in commercial Pt–Ru/C is 34%, it is only 23% in the in-house made catalyst, which further decreases to 18% on air annealing beyond 200 °C. The concentration of oxidized species in the in-house catalyst remains unaltered up to 200 °C, but the oxidized species increase at the cost of metallic phase on heating at temperatures >200 °C.

The surface concentration ratios of Ru to Pt in the Pt–Ru/C catalysts were calculated employing the following relation [13]:

$$\frac{X_{\mathrm{Ru}}}{X_{\mathrm{Pt}}} = \frac{I_{\mathrm{Ru}}\sigma_{\mathrm{Pt}}\lambda_{\mathrm{Pt}}D_{\mathrm{E}}(\mathrm{Pt})}{I_{\mathrm{Pt}}\sigma_{\mathrm{Ru}}\lambda_{\mathrm{Ru}}D_{\mathrm{E}}(\mathrm{Ru})} \quad (8)$$

where X, I, σ, λ and D_{E} are the surface concentration, intensity, photoionization cross-section, mean escape depth and geometric factor, respectively. Integrated intensities of Ru($3p_{3/2}$) and Pt(4f) core level peaks have been taken into account to estimate the concentration. Photoionization cross-sections and mean escape depths have been obtained from the literature [13,14]. The Ru/Pt ratio is 0.93 for the commercial catalyst; it is ∼0.95 for the as-prepared and heat-treated catalysts up to 200 °C, but increases to 1 for the catalyst air-annealed at 250 °C for half-an-hour. Accordingly, only a little surface enrichment of Ru takes place on its air annealing.

The k^3-weighted Fourier transforms for the Pt/C, commercial Pt–Ru/C, as-prepared Pt–Ru/C catalyst and Pt–Ru/C catalysts annealed at 200, 250 and 300 °C are shown in Fig. 10(a)–(f), respectively. The solid lines indicate best fit to the data. Fourier transform (FT) for Pt/C sample shows peaks due to Pt–O correlation at about 1.7 Å (phase un-corrected value) and Pt–Pt correlation in the range between 2 and 3 Å. The Pt–Ru catalyst samples show a two-peak structure due to interference of backscattered of X-ray photons from Pt and Ru neighbours around the absorbing Pt atom. The presence of such a two-peak structure indicates Pt–Ru alloy formation in these catalysts [15]. A comparison of X-ray diffraction patterns for Pt–Ru/C and Pt/C catalysts clearly indicates a shift in the (1 1 1) peak to a higher angle in the Pt–Ru/C sample indicating the contraction of lattice due to alloy formation [10].

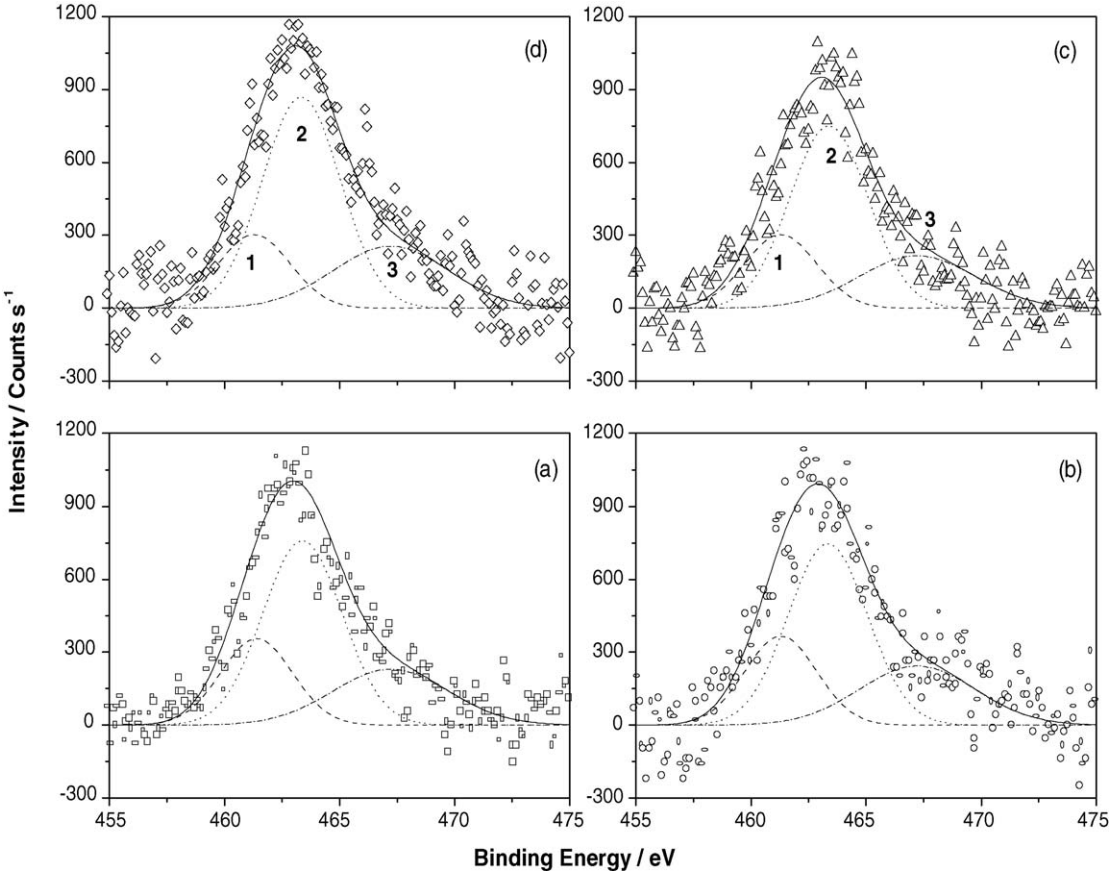

Fig. 9. Ru($3p_{3/2}$) region in (a) as-prepared Pt–Ru/C and as-prepared Pt–Ru/C after annealing it in air at (b) 200 °C; (c) 250 °C; (d) 300 °C (species 1, 2, 3 correspond to Ru^0, RuO_2, and $RuO_2{\cdot}xH_2O$, respectively).

Table 3
Structural parameters of Pt/C, commercial Pt–Ru/C, as-prepared Pt–Ru/C and air annealed Pt–Ru/C catalysts as obtained from EXAFS analysis

Sample	Bond	Coordination number	Bond length (Å)	σ^2 (Å^2)
Pt/C	Pt—O	1.9 (4)	1.993 (7)	0.007 (1)
	Pt—Pt	6.1 (2)	2.764 (4)	0.006 (1)
	Pt—Pt	2.3 (5)	3.91 (2)	0.007 (1)
Pt–Ru/C (commercial)	Pt—O	1.2 (3)	2.016 (9)	0.004 (2)
	Pt—Pt	4.9 (3)	2.750 (9)	0.008 (1)
	Pt—Ru	2.4 (6)	2.736 (8)	0.006 (2)
Pt–Ru/C (as-prepared)	Pt—O	2.1 (2)	2.033 (9)	0.011 (1)
	Pt—Pt	4.5 (3)	2.732 (4)	0.008 (1)
	Pt—Ru	0.60 (7)	2.717 (7)	0.004 (1)
Pt–Ru/C (200 °C)	Pt—O	1.6 (1)	2.018 (6)	0.006 (1)
	Pt—Pt	3.6 (2)	2.744 (3)	0.007 (1)
	Pt—Ru	0.77 (8)	2.751 (7)	0.006 (1)
Pt–Ru/C (250 °C)	Pt—O	1.6 (1)	2.024 (5)	0.006 (1)
	Pt—Pt	4.9 (2)	2.744 (2)	0.008 (1)
	Pt—Ru	1.0 (1)	2.738 (6)	0.007 (1)
Pt–Ru/C (300 °C)	Pt—O	1.5 (1)	2.018 (5)	0.006 (1)
	Pt—Pt	4.9 (2)	2.748 (2)	0.008 (1)
	Pt—Ru	1.0 (1)	2.754 (6)	0.007 (1)

Figures in brackets 3rd, 4th and 5th columns are standard deviation.

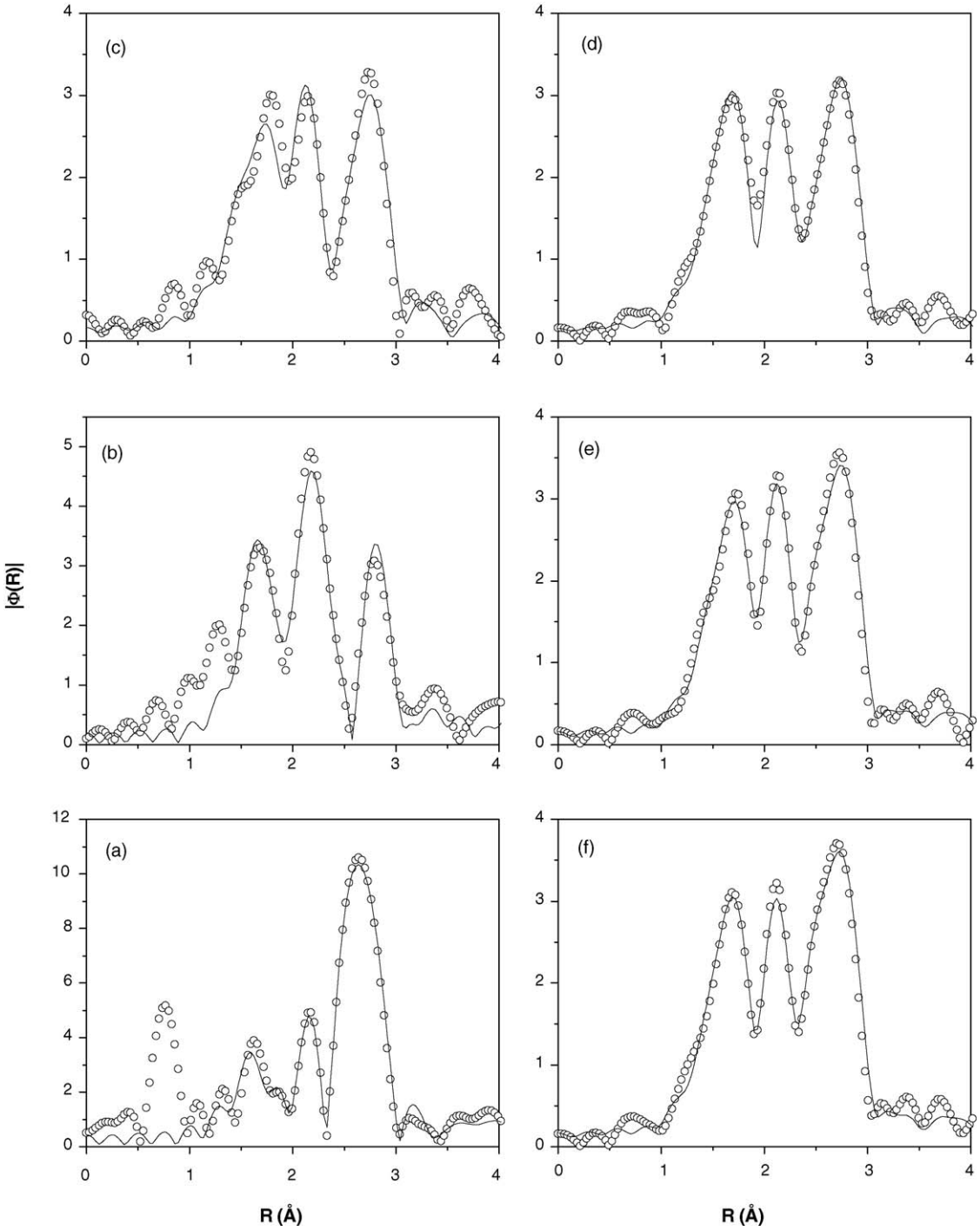

Fig. 10. Magnitude of Fourier transform of EXAFS at Pt L_3 edge in (a) Pt/C, (b) commercial Pt–Ru/C, (c) as-prepared Pt–Ru/C and as-prepared Pt–Ru/C after annealing it in air at (d) 200 °C; (e) 250 °C; (f) 300 °C. Solid line indicates best fit to the data.

Curve fitting results and the fitted parameters for all the samples are presented in Fig. 11(a)–(f) and Table 3. The backscattering amplitudes for Pt–Pt and Pt–Ru were calculated using FEFF 6.01 program for fcc Pt–Ru alloy and Pt–O correlation was estimated from FEFF calculation for PtO_2. The presence of a Pt–O correlation indicates that the surface Pt atoms are oxidized. A fitting to this peak gives a bond length of about 2 Å, which is larger than the Pt–O bond length in PtO_2. XPS results also support that a fraction of total Pt is in 2+/4+ states. The Pt–Pt and Pt–Ru bond lengths obtained for Pt–Ru samples are smaller than the Pt–Pt bond length in metallic Pt. This indicates that Pt and Ru atoms in Pt–Ru are not randomly distributed although the average crystal structure is fcc implying thereby a formation of ordered Pt–Ru alloy [2]. The smaller coordination numbers (*N*) and bond distances (*R*) for the supported particles as compared to Pt

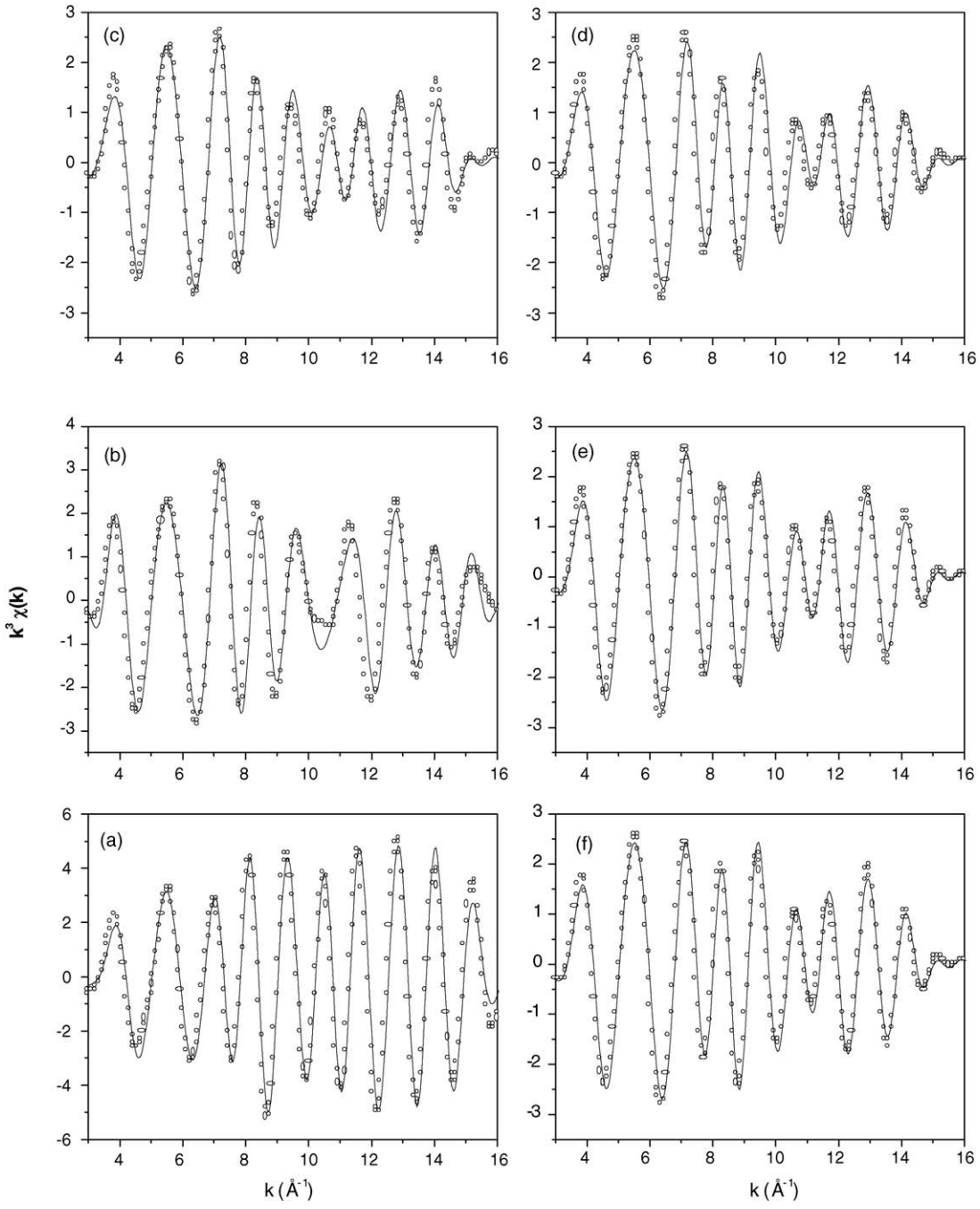

Fig. 11. The k^3-weighted inverse Fourier transform for (a) Pt/C, (b) commercial Pt–Ru/C, (c) as-prepared Pt–Ru/C and as-prepared Pt–Ru/C after annealing it in air at (d) 200 °C; (e) 250 °C; (f) 300 °C. Solid line indicates best fit to the data.

foil ($N = 12$ and $R = 2.779$ Å) are consistent with the small size of the particles and other EXAFS studies [9,15,16]. The fits also indicate that, in all the Pt–Ru/C catalysts, only a little Ru is in the first coordination shell. For icosahedral or cuboctahedral particles of about 5 nm in diameter, the percentage of the Pt atoms that are on the surface is approximately 50. Thus, the Pt–Ru/C sample may comprise a Pt core with less than a full monolayer of Ru on the surface, or it may have a mixed system with less than the stoichiometric quantity of Ru in the particle [15,16].

It is noteworthy that in our tailored Pt–Ru samples, annealing plays an important role in deciding the local structure around Pt atoms. The number of oxygen neighbours (N_O) as well as their distance from the Pt ion ($R_{Pt–O}$) remains approximately same but for the as-prepared sample where both N_O and $R_{Pt–O}$ are slightly higher. The bond distance between Pt and Ru ($R_{Pt–Ru}$) and its coordination number (N_{Ru}) both change with annealing temperature. In the as-prepared sample, 4.5 Pt and 0.6 Ru neighbours are at a distance of 2.732 and 2.717 Å, respectively. By contrast, Pt in the commercial sam-

ple has a higher number of Pt and Ru neighbours (Table 3). The coordination number of Pt and Ru also increases except for the sample annealed at 200 °C. In this case, the Pt–Pt coordination number decreases to 3.6 from 4.5 in the as-prepared sample. This may be due to the formation of some sort of a meta-stable state at 200 °C. The surface ratio of Ru to Pt obtained from XPS also decreases from 95 to 94%, which would mean the surface to grow more Pt rich. XRD pattern of the sample annealed at 200 °C also has more distinct peaks in relation to other samples. For the samples annealed at 250 and 300 °C, both the Pt–Pt and Pt–Ru coordination numbers increase as compared to their values obtained in the as-prepared sample. Annealing at 200 °C and above, however, results in increased Pt–Pt and Pt–Ru bond lengths, which tend to equalize. Thus, annealing stabilizes the Pt–Ru alloy formation in the Pt–Ru samples.

Such an intimate contact between Pt and Ru for alloy stabilization is seminal to electro-oxidation of methanol. The methanol electro-oxidation reaction is a slow process involving six-electron transfer for complete oxidation to CO_2. Various reaction intermediates that are CO-like species are formed during electro-oxidation, which irreversibly adsorb on the Pt surface and poison the catalyst. To oxidize the methanolic residue adsorbed on the Pt surface, H_2O needs to be discharged on adjacent Ru atom at a potential close to methanol oxidation (0.2 V versus SHE) resulting in Ru–OH species, which are responsible to oxidize the methanolic residue according to Eq. (7) [3,4]. Since the as-prepared Pt–Ru/C contains more of oxidized Pt with a lower Ru co-ordination number (Table 3), it exhibits poor methanol-oxidation kinetics in relation to heat-treated Pt–Ru/C catalysts. In case of commercial Pt–Ru/C catalyst, although Pt and Ru coordination numbers are higher, the Pt–Pt and Pt–Ru distances are unequal, which could be a reason for its lower methanol-oxidation activity at current densities >350 mA cm^{-2}. We therefore conjecture that increased coordination number for Pt and Ru around Pt, and almost equal Pt–Pt and Pt–Ru bonds for our air annealed Pt–Ru/C catalyst samples at temperatures between 250 and 300 °C seem to be responsible for increased electro-oxidation of methanol in relation to both the as-prepared and commercial Pt–Ru/C catalyst samples.

4. Conclusions

XPS studies on our as-prepared and air-annealed Pt–Ru/C catalyst reflect that, during air annealing of the as-prepared Pt–Ru/C catalyst, Ru metal from the bulk catalyst diffuses to the catalyst surface increasing the oxidic ruthenium content on the catalyst surface. EXAFS studies on Pt–Ru/C catalyst suggest that during the air annealing of Pt–Ru/C catalyst an ordered Pt–Ru alloy formation is promoted. These findings have important implications for the electrochemical oxidation of methanol on Pt–Ru/C catalyst since during the methanol oxidation reaction the catalyst is operated in a potential regime in which oxides should not be present but where supply of oxygen is of paramount importance.

Acknowledgements

Financial assistance from the Council of Scientific and Industrial Research, New Delhi is gratefully acknowledged. We thank Dr. R.A. Mashelkar, FRS for his keen interest and encouragement.

References

[1] A.K. Shukla, C.L. Jackson, K. Scott, R.K. Raman, Electrochim. Acta 47 (2002) 3401.
[2] M. Watanabe, M. Uchida, S. Motoo, J. Electroanal. Chem. 229 (1987) 395.
[3] M.P. Hogarth, T.R. Ralph, Platinum Met. Rev. 46 (2002) 146.
[4] A.S. Aricò, S. Srinivasan, V. Antonucci, Fuel Cells 1 (2001) 1.
[5] J. Wong, F.W. Lytle, R.P. Messner, D.H. Maylor, Phys. Rev. B 30 (1984) 5596.
[6] E.A. Stern, M. Newville, B.D. Ravel, Y. Yacobi, D. Haskel, Phys. B 208/209 (1995) 117.
[7] S.I. Zabinski, J.J. Rehr, A. Ankudinov, R.C. Albers, M.J. Eller, Phys. Rev. B 52 (1995) 2995.
[8] A.S. Aricò, V. Baglio, A. Di Blasi, E. Modica, P.L. Antonucci, V. Antonucci, J. Electroanal. Chem. 557 (2003) 167.
[9] A.K. Shukla, R.K. Raman, N.A. Choudhury, K.R. Priolkar, P.R. Sarode, S. Emura, R. Kumashiro, J. Electroanal. Chem. 563 (2004) 181.
[10] E.M. Crabb, M.K. Ravikumar, D. Thompsett, M. Hurford, A. Rose, A.E. Russell, Phys. Chem. Chem. Phys. 6 (2004) 1792.
[11] P. Bera, K.R. Priolkar, A. Gayen, P.R. Sarode, M.S. Hegde, S. Emura, R. Kumashiro, V. Jayaram, G.N. Subbanna, Chem. Mater. 15 (2003) 2049.
[12] D.R. Rolison, P.L. Hagans, K.E. Swider, J.W. Long, Langmuir 15 (1999) 774.
[13] D.R. Penn, J. Electron Spectrosc. Relat. Phenom. 9 (1976) 29.
[14] J.H. Scofield, J. Electron Spectrosc. Relat. Phenom. 8 (1976) 129.
[15] A.E. Russell, S. Maniguet, R.J. Mathew, J. Yao, M.A. Roberts, D. Thompsett, J. Power Sources 96 (2001) 226.
[16] S. Mukerjee, R.C. Urian, Electrochim. Acta 47 (2002) 3219.